

**ANALYSIS OF YTTRIUM IRON GARNET (YIG)  
RESONATOR WITH EXCESS  $\text{Fe}_2\text{O}_3$  FOR  
WIDEBAND ANTENNA APPLICATIONS**

**MOHAMADARIFF OTHMAN**

**UNIVERSITI SAINS MALAYSIA**

2015

**ANALYSIS OF YTTRIUM IRON GARNET (YIG)  
RESONATOR WITH EXCESS  $\text{Fe}_2\text{O}_3$  FOR  
WIDEBAND ANTENNA APPLICATIONS**

**by**

**MOHAMADARIFF OTHMAN**

**Thesis submitted in fulfillment of the requirements  
for the degree of  
Doctor of Philosophy**

**June 2015**



## **ACKNOWLEDGEMENT**

First and foremost, praise be to ALLAH, the most gracious and the most merciful. Without His blessing and guidance my accomplishments would never have been possible. I would like to express my deepest gratitude to my advisor, Associate Professor Dr. Mohd Fadzil Ain and co-supervisor, Professor Zainal Arifin Ahmad for their excellent guidance, caring, patience, and providing me with an excellent atmosphere for doing research. Their guidance helped me in all the time of research and writing of this thesis. I could not have imagined having better advisors and mentors for my Ph.D study. I am greatly indebted to my wife Wan Zulaikha Wan Hamidon. She was always there cheering me up and not letting me give up. This I cannot thank her enough. I also want to thank my children: Alif and Ameen. I specially want to thank my parents and parents-in-law for supporting me spiritually throughout my life. Further thanks to members of my research group, both present and past. Thank you to Dr Ali Othman, Dr Asari Sulaiman, Dr Yazeed Qasaymeh, Dr Seyi, Wan Fahmin Faiz, Nik Akmar Rejab, Mohd Azman Zakariyya, Ihsan Ahmad Zubir, Kang Chia Chao, Ubaid Ullah, Khairul Anuar, Muhammad Fathul Najmi and Zulaimi Zahar. My sincere thanks also goes to technicians; Mr. Abdul Latip Hamid, Mr Elias Zainuddin and Mdm Zammira Khairuddin for their assistance and providing technical support in the Communications and PCB laboratory. I would like also to thank Universiti Sains Malaysia (USM) and Ministry of Higher Education (MOHE) for providing the opportunity and supporting my research project through USM RUT 1001/PELECT/854004, USM PRGS 1001/PELECT/8044046 and Mybrain15 KPT (B) 831219045295.

# TABLE OF CONTENTS

<b>ACKNOWLEDGEMENT.....</b>	<b>ii</b>
<b>TABLE OF CONTENTS.....</b>	<b>iii</b>
<b>LIST OF TABLES.....</b>	<b>ix</b>
<b>LIST OF FIGURES.....</b>	<b>xxi</b>
<b>LIST OF SYMBOLS.....</b>	<b>xv</b>
<b>LIST OF ABBREVIATIONS.....</b>	<b>xvii</b>
<b>ABSTRAK.....</b>	<b>xix</b>
<b>ABSTRACT.....</b>	<b>xxiii</b>
<b>CHAPTER 1.....</b>	<b>1</b>
1.1 Overview .....	1
1.2 Problem statement.....	3
1.3 Objectives of research .....	6
1.4 Scope of Research .....	7
1.5 Contributions.....	8
1.6 Thesis Organization .....	9
<b>CHAPTER 2.....</b>	<b>10</b>
2.1 Dielectric Resonator.....	10
2.1.1 Introduction .....	10

2.1.2	Major Features .....	11
2.1.3	Methods of Coupling .....	13
2.1.4	The Significance of Electromagnetic Field Pattern .....	15
2.1.5	Excited Modes Using Microstrip line Coupling .....	17
2.2	YIG Resonator .....	23
2.2.1	Overview .....	23
2.2.2	YIG and $\text{Fe}_2\text{O}_3$ Excess .....	25
2.2.3	Solid State Reaction .....	27
2.2.4	Characterization .....	29
2.2.4.1	X-Ray Diffraction (XRD) .....	29
2.2.4.2	Field Emission Scanning Electron Microscopy (FESEM) ..	30
2.2.4.3	High Frequency Characterization .....	30
2.3	Properties of YIG Resonator .....	31
2.3.1	Permittivity and Permeability .....	31
2.3.2	Loss Tangent .....	34
2.3.3	Quality Factor and Bandwidth .....	35
2.4	YIG Resonator in Antenna Application .....	38
2.4.1	YIG Resonator Advantages .....	38
2.4.2	YIG Resonator as Antenna .....	41
2.4.3	YIG Resonator Antenna Related Works .....	43
2.5	Analysis of YIG Resonator Antenna (YRA) .....	45
2.5.1	Introduction .....	45
2.5.2	Numerical methods .....	46

2.5.3	Theoretical models .....	47
2.5.3.1	Dielectric Waveguide .....	47
2.5.3.2	Magnetic Wall Model (MWM) .....	48
2.5.3.3	Curve Fitting Model (CFM) .....	51
2.5.4	MWM versus CFM .....	56
2.6.	Statistical Analysis in Antenna .....	58
2.6.1	Method of Least Squares.....	58
2.6.2	Correlation and Regression Analysis .....	59
2.6.3	Hypothesis Testing.....	62
2.7	Wideband YIG Resonator Antenna .....	66
2.7.1	Introduction .....	66
2.7.2	Wideband Techniques in DRA .....	66
2.7.3	Design Procedure of Cylindrical YRA .....	74
2.7.4	Arrangement of Stacked YRA .....	76
2.7.5	Effective Permittivity of Stacked YRA .....	77
2.8	Summary .....	79
<b>CHAPTER 3.....</b>		<b>81</b>
3.1	The Design Specifications.....	81
3.2	Preparation of YIG Resonator with different excess $\text{Fe}_2\text{O}_3$ .....	84
3.2.1	Composition Preparation.....	84
3.2.2	Mixing and Milling .....	85
3.2.3	Calcination .....	86

3.2.4	Pressing .....	86
3.2.5	Sintering .....	87
3.3	Dielectric Characterization of YIG Resonator .....	88
3.3.1	Field Emission Scanning Electronic Microscope (FESEM) .....	88
3.3.2	X-ray Diffraction Machine (XRD) .....	89
3.3.3	Permittivity and Loss Tangent .....	89
3.4	Modification of Curve Fitting Equations .....	92
3.5	Verification of Modified Curve Fitting Equation .....	93
3.6	Design of Wideband Stacked YIG Antenna .....	96
3.6.1	Operational Frequency and Bandwidth .....	96
3.6.2	Feeder .....	97
3.6.3	Dimension of YIG antenna .....	101
3.6.4	Number of Stacked YIG Resonators .....	103
3.6.5	Optimum Combination in Stacked Configuration .....	104
3.7	YIG Antenna Simulation using CST Microwave Studio .....	105
3.7.1	Introduction .....	105
3.7.2	General Setting of CST .....	106
3.7.3	Configuration of CST for Wideband Stacked YIG Antenna .....	108
3.8	Measurements of the YIG Antenna .....	110
3.8.1	Introduction .....	110
3.8.2	S-Parameter ( $S_{11}$ ) measurement .....	111
3.8.3	Antenna Radiation Pattern Measurement .....	112



3.8.4	Antenna Gain Measurement.....	115
3.9	Summary .....	116
<b>CHAPTER 4.....</b>		<b>117</b>
4.1	XRD and SEM Analysis .....	117
4.2	Permittivity and Loss Tangent of YIG Resonator .....	122
4.3	Modified Curve Fitting Equation .....	126
4.3.1	Correlation Analysis .....	127
4.3.2	Regression Analysis .....	128
4.4	Verification of Modified Curve Fitting Equation .....	132
4.4.1	Resonant Frequency .....	134
4.4.2	Q factor .....	137
4.5	Designing a Wideband Stacked YIG Antenna for 17.3 to 21.2 GHz .....	138
4.5.1	Introduction .....	138
4.5.3	Dimension of YIG Antenna .....	139
4.5.4	Number of Stacked Resonators .....	140
4.5.5	Optimum Combination for Stacked Configuration.....	143
4.6	Wideband Stacked YIG antenna for 17.3 GHz to 21.1 GHz application .....	147
4.6.1	Optimization of YIG resonators combination.....	147
4.6.2	Load Impedance of Stacked YIG Antenna .....	151
4.6.3	Reflection Coefficient of Stacked YIG Antenna .....	153
4.6.4	Radiation Pattern.....	156

4.6.5	Gain.....	159
4.7	Analysis on Wideband Stacked YIG antenna .....	160
4.7.1	Effect of Adjusting YRA Placement on Microstrip line to $S_{11}$ .....	160
4.8	Summary .....	167
<b>CHAPTER 5.....</b>		<b>169</b>
5.1	Overall Conclusion.....	169
5.2	Future Works.....	171
<b>REFERENCES.....</b>		<b>172</b>
<b>LIST OF PUBLICATIONS.....</b>		<b>185</b>
<b>APPENDICES.....</b>		<b>186</b>

## LIST OF TABLES

Table 2.1	List of coupling methods for DR	13
Table 2.2	Difference between Curve Fitting Model (CFM) and Magnetic Wall Model (MWM)	57
Table 2.3	Literature reviews related to the MWM and CFT techniques	57
Table 2.4	List of techniques for DRA bandwidth enhancement	
Table 2.5	Bandwidth improvement technique in multiple DRA	72
Table 3.1	Preparation of standard 20 gm YIG stoichiometry (0 % excess $\text{Fe}_2\text{O}_3$ )	85
Table 3.2	Preparation of addition excess $\text{Fe}_2\text{O}_3$ (wt%) into YIG stoichiometry	85
Table 3.3	Variables of least square method	92
Table 4.1	Percentages of YIG, YIP and Hematite phases in YIG Resonator	119
Table 4.2	List of $\epsilon_r$ for YIG resonator with various excess $\text{Fe}_2\text{O}_3$	124
Table 4.3	Comparison of resonant frequency and Q factor of $\text{HE}_{11}$ mode for YR with $r = 5$ mm and $h = 1$ mm	131
Table 4.4	Two sided t test for resonant frequency using Minitab	131
Table 4.5	Two sided t test for Q factor using Minitab	134
Table 4.6	Potential height for YIG resonator antenna	137
Table 4.7	Classifications of YIG resonators	141
Table 4.8	List of combination of YIG resonators with different excess $\text{Fe}_2\text{O}_3$ for (a) $X_2 + X_3 = 30$ , $x_{eff} = 12.67$ , (b) $X_2 + X_3 = 31$ , $x_{eff} = 13$ , (c) $X_2 + X_3 = 32$ , $x_{eff} = 13.33$	143
Table 4.9	Comparison of Design A, Design B and Design C	147
Table 4.10	Comparison of Design D, Design E and Design F	147

Table 4.11	Comparison of Design H, Design I and Design J	148
Table 4.12	Comparison of simulated and measured load impedance, $Z_L$	149
Table 4.13	Comparison between the simulated and measured wideband YIG antenna	151

## LIST OF FIGURES

Figure 2.1	Cylindrical dielectric resonator structure	11
Figure 2.2	Methods of coupling (a) Probe coupling, (b) Slot coupling, (c) Microstrip line coupling, (d) Coplanar waveguide coupling, (e) Dielectric image guide (DIG) coupling	14
Figure 2.3	Microstrip line coupling of DRA with varactor diode.	16
Figure 2.4	Mode suppression method to $HE_{11}$ mode.	17
Figure 2.5	Method of coupling to $TE_{01}$ DR	18
Figure 2.6	Field distribution of the $TE_{01\delta}$ mode: (a) $H_x$ and $H_y$ at $z = 0$ ; (b) $E_y$ and $E_z$ at $x = 0$	19
Figure 2.7	Method of coupling to $TM_{01}$ DR	20
Figure 2.8	Coupling to $HE_{11}$ mode: (a) microstrip line; (b) probe and slot coupling to $HE_{11}$ mode	21
Figure 2.9	Field distribution of $HE_{11\delta}$ mode: (a) $H_x$ and $H_y$ at $z = 0$ ; (b) $E_y$ and $E_z$ at $x = 0$	22
Figure 2.10	Crystal structure of YIG garnet	24
Figure 2.11	Conventional solid state reaction steps	28
Figure 2.12	Coaxial probe characterization method	31
Figure 2.13	Loss tangent vector diagram	34
Figure 2.14	Rectangular YRA with electromagnetic source	41
Figure 2.15	Geometry of cylindrical dielectric antenna	43
Figure 2.16	Dielectric body of revolution	52
Figure 2.17	Moment matrix determinant ( $m=0$ ) along imaginary axis of complex frequency plane for dielectric cylinder with $\epsilon=35$ , $a=5$ mm, and $h=5$ mm	54

Figure 2.18	Curve fitting technique in statistical analysis	59
Figure 2.19	Linear regression line	62
Figure 2.20	T-Statistic Two-Sides for p-value less than significance level of 5%	65
Figure 2.21	Dual band and wideband characteristic for two-DRA configuration (a) Dual bands: $(\Delta f_u + \Delta f_l) = 2 (f_u - f_l)$ (b) Dual bands: $(\Delta f_u + \Delta f_l) < 2 (f_u - f_l)$ (c) Wideband: $(\Delta f_u + \Delta f_l) > 2 (f_u - f_l)$	69
Figure 2.22	Embedded and stacked wideband DRA	70
Figure 2.23	Cylindrical YRA designs	75
Figure 2.24	Dimension (cm) of the cylindrical DRAs with $\epsilon_r = 15$	76
Figure 2.25	Three layers stacked configuration: (a) microstrip line; (b) slot, probe and coplanar waveguide.	77
Figure 2.26	Effective $\epsilon_r$ of YIG resonator	78
Figure 3.1	Spectrum allocation of Malaysia (a) required frequency range (b) defining of color	82
Figure 3.2	Research methodology flowchart	83
Figure 3.3	Calcination profile for YIG powder	86
Figure 3.4	YIG sintering profile at temperature of 1420 °C for 6 hours	87
Figure 3.5	Proper dimension of DUT for characterization using 85070E Dielectric Probe Kit and Network Analyzer	90
Figure 3.6	Steps of dielectric probe calibration a) air; b) short; and c) water	90
Figure 3.7	Regression analysis model setting in Minitab	92
Figure 3.8	Transmission line of proposed YIG antenna	96
Figure 3.9	Length of microstrip line for the proposed YIG antenna	100
Figure 3.10	Effective excess $\text{Fe}_2\text{O}_3$ in stacked YIG structure (Rashidian et al., 2005).	104

Figure 3.11	Microstrip line feeder configuration.	105
Figure 3.12	Waveguide port of YIG Resonator antenna	106
Figure 3.13	Boundary condition of YIG Resonator antenna	107
Figure 3.14	Simulated stacked YIG antenna: (a) Three YIG resonators; (b) Simulated structure of wideband stacked YIG antenna; (c) Coupling optimization of the YIG antenna.	108
Figure 3.15	Measured stacked YIG antenna: (a) Fabricated YIG resonators; (b) Measured structure of YIG antenna.	109
Figure 3.16	PNA-X network analyzer for S-parameter measurement.	110
Figure 3.17	Radiation pattern and gain measurement set up in anechoic chamber	112
Figure 3.18	Placement of antenna under test for radiation pattern and gain measurement: (a) H-plane; (b) E-plane.	112
Figure 4.1	XRD pattern of YIG sample with various excess $\text{Fe}_2\text{O}_3$	116
Figure 4.2	SEM images of YIG sample with various excess $\text{Fe}_2\text{O}_3$	118
Figure 4.3	Characterization of $\epsilon_r$ for YIG resonator with various excess $\text{Fe}_2\text{O}_3$	121
Figure 4.4	Characterization of tangent $\delta$ for YIG Resonator with various excess $\text{Fe}_2\text{O}_3$	123
Figure 4.5	Scatter plot of data, cubic, quadratic, linear model against $\text{Fe}_2\text{O}_3$ excess	126
Figure 4.6	Cubic-type regression model with best fit equation	127
Figure 4.7	p-value of the modified resonant frequency equation of $\text{HE}_{11}$ mode	130
Figure 4.8	p-value of the modified Q factor equation of $\text{HE}_{11}$ mode	130
Figure 4.9	Statistic of t-distribution if the null hypothesis is true.	133
Figure 4.10	Cylindrical YIG resonator antenna designs	137

Figure 4.11	Acceptable bandwidth of YIG with excess $\text{Fe}_2\text{O}_3$	139
Figure 4.12	Proposed stacked YIG antenna arrangement with microstrip line feeder based on excess $\text{Fe}_2\text{O}_3$ .	141
Figure 4.13	Optimization of YR combinations for $X_2 + X_3 = 30$	146
Figure 4.14	Optimization of YR combinations for $X_2 + X_3 = 31$	146
Figure 4.15	Optimization of YR combinations for $X_2 + X_3 = 32$	147
Figure 4.16	Simulated and measured load impedance, $Z_L$ of YIG antenna	149
Figure 4.17	Simulated and measured return loss of stacked YIG antenna.	151
Figure 4.18	E-field distribution of YIG antenna at a) 17.2 GHz, b) 19.34 GHz and c) 20.9 GHz.	152
Figure 4.19	Simulated and measured radiation pattern in E and H-planes at a) 17.2 GHz, b) 18.2 GHz, c) 19.2 GHz and d) 20.9 GHz.	155
Figure 4.20	Gain measurement	156
Figure 4.21	Effect of variation of s distance to return loss	158
Figure 4.22	Surface current distribution of stacked YIG antenna at $s = 3$ mm a) 17.2 GHz, b) 19.34 GHz and c) 20.9 GHz.	159
Figure 4.23	Effect of YR17 (top layer) thickness variation to $S_{11}$	160
Figure 4.24	Effect of YR14 (middle layer) thickness variation to $S_{11}$	161
Figure 4.25	Effect of YR8 (bottom layer) thickness variation to $S_{11}$	161
Figure 4.26	Effect of YR17 (top layer) permittivity variation to $S_{11}$	163
Figure 4.27	Effect of YR14 (middle layer) permittivity variation to $S_{11}$	163
Figure 4.28	Effect of YR8 (bottom layer) permittivity variation to $S_{11}$	164



## LIST OF SYMBOLS

$\mu_r$	Permeability
$\varepsilon_r$	Permittivity
$\varepsilon_{eff}$	Effective Permittivity
$M$	Permeability
$\mu_{eff}$	Effective Permeability
Tan $\delta$	Loss Tangent
$D$	Dissipation Factor
$P$	Dissipated Power
$W$	Total Stored Energy
$\Omega$	Ohms (Impedance)
$\beta$	Phase Constant
$\gamma$	Propagation Constant
$K$	Coupling Coefficient
$R^2$	Coefficient of Determination
$R$	Coefficient of Correlation
$S$	Standard Deviation
$\Gamma$	Reflection Coefficient
$\omega$	Angular Resonant Frequency
$F$	Resonant Frequency
$f_{cen}$	Center Frequency

$\lambda_0$	The Wavelength in Free Space
$\lambda_g$	The Guided Wavelength
$c$	Speed of Light
$k_o$	The Free-Space Wave Number
$k_x$	Wave Number in x Direction
$k_y$	Wave Number in y Direction
$k_z$	Wave Number in z Direction
$Z_o$	Characteristic Impedance
$Z_{in}$	Input Impedance
$Z_L$	Load Impedance
$R_L$	Load Resistance
$X_L$	Load Reactance

## LIST OF ABBREVIATIONS

AUT	Antenna Under Test
$\Delta B$	Impedance Bandwidth
CFM	Curve Fitting Model
CST	Computer Simulation Technology
DWM	Dielectric Waveguide Model
DR	Dielectric Resonator
DRA	Dielectric Resonator Antenna
dB	Decibel
3-D	Three Dimensions
E-field	Electric Field
H-field	Magnetic Field
GHz	Giga Hertz
HPBW	Half Power Beamwidth
HE	Hybrid Electromagnetic
Mm	Milli-meter
MWS	Microwave Wave Studio
RF	Radio Frequency
FESEM	Field Emission Scanning Electronic Microscope
SLL	Side Lobe Level
TEM	Transverse Electromagnetic
TE	Transverse Electric
TM	Transverse Magnetic

XRD	X-ray Diffraction
YIG	Yttrium Iron Garnet
YRA	YIG Resonator Antenna
YRX	YIG Resonator with X % Amount of Excess $\text{Fe}_2\text{O}_3$
YUT	YIG Under Test

# **ANALISIS TERHADAP PENYALUN YTTRIUM IRON GARNET (YIG) DENGAN LEBIHAN $\text{Fe}_2\text{O}_3$ BAGI APLIKASI ANTENA JALUR LEBAR**

## **ABSTRAK**

Komunikasi satelit memainkan peranan penting dalam bidang telekomunikasi. Menyedari hakikat ini, antena jalur lebar adalah sebahagian daripada penyelesaian untuk mewujudkan konsep penggunaan frekuensi lebar dalam teknologi satelit. Antena penyalun dielektrik (DRA) jalur lebar menyediakan kecekapan yang lebih baik dan pengecilan saiz berbanding antena logam. Walau bagaimanapun, penyalun dielektrik (DR) dengan ketelusan ( $\epsilon_r$ ) dan saiz yang berbeza menyumbang kepada peningkatan dalam kerumitan reka bentuk dan fabrikasi DRA. Selain itu, setiap kali menggunakan bahan dielektrik baru, ia mesti dicirikan sepenuhnya. Pencirian ini dianggap berulang sebelum analisis DRA itu dijalankan. Oleh itu, tujuan kajian ini adalah untuk merealisasikan antena jalur lebar berkesan dan analisis antena yang lebih pantas. Penambahbaikan kepada DRA jalur lebar dibuat dengan menggunakan bahan yttrium iron garnet (YIG) berketelusan rendah dengan lebihan  $\text{Fe}_2\text{O}_3$  tanpa pemincangan arus terus untuk menghasilkan penyalun silinder dengan dimensi yang sama tetapi  $\epsilon_r$  berbeza. Penyalun YIG (YR) telah dibangunkan dengan menggunakan kaedah tindak balas keadaan pepejal dan dicirikan dengan pembelauan sinar-X (XRD), mikroskop lepasan lapangan imbasan elektron (FESEM) dan kit kuar dielektrik (Agilent 85070E). Berdasarkan keputusan pencirian, model lengkung sesuai (CFM) telah diubahsuai menggunakan perisian Minitab berdasarkan kepada analisis korelasi dan regresi.

Simulasi struktur YRA ini dibuat menggunakan perisian teknologi simulasi komputer studio gelombang mikro (CST), manakala pengukuran parameter-S menggunakan PNA-X Network Analyzer (8720D). Corak radiasi YRA telah juga diuji dengan menggunakan kebuk tanpa gema yang berukuran 10 meter. Analisis XRD dan SEM memberi petunjuk kepada tindak balas sepenuhnya, kepadatan dan kepejalan silinder YIG menggunakan kaedah keadaan pepejal. Penggunaan lebihan  $\text{Fe}_2\text{O}_3$  yang berbeza menghasilkan YIG dengan  $\epsilon_r$  rendah dalam julat 10.04 ke 17.36 dengan kehilangan tangen ( $\tan \delta$ ) yang rendah. Korelasi antara  $\epsilon_r$  dan lebihan  $\text{Fe}_2\text{O}_3$  digunakan untuk mengubahsuai persamaan lengkung sesuai. Persamaan yang diubah memberikan analisis yang cepat pada YRA dengan memasukkan kehadiran lebihan  $\text{Fe}_2\text{O}_3$  dan bukannya nilai  $\epsilon_r$ . Pekali korelasi dengan -0.862 menunjukkan hubungan yang kuat antara  $\epsilon_r$  dan lebihan  $\text{Fe}_2\text{O}_3$ . Pekali penentuan,  $R^2$  sebanyak 99.6% menunjukkan bahawa persamaan yang dihasilkan adalah sangat sesuai dengan data  $\epsilon_r$ . Pengujian hipotesis dengan nilai p yang tinggi melebihi 99% mengesahkan bahawa persamaan yang diubahsuai adalah sama dengan persamaan asal. Penyalun YIG yang dihasilkan dan persamaan yang diubahsuai digunakan bersama untuk membentuk antenna penyalun YIG (YRA) berjalur lebar bertindan. Tiga YIG disusun dengan kombinasi lebihan  $\text{Fe}_2\text{O}_3$  yang berbeza bagi menghasilkan antenna jalur lebar yang dicadangkan. Penyalun YIG dengan 8% (YR8), 14% (YR14) dan 17% (YR17) lebihan  $\text{Fe}_2\text{O}_3$  menghasilkan gabungan YR yang terbaik dengan frekuensi masing-masing adalah 17.25 GHz, 19.18 GHz dan 20.81 GHz. Kesan gabungan daripada tiga penyalun YIG menghasilkan lebar jalur dengan 24.22% diukur daripada -10 dB galangan jalur lebar berpusat di 19.25 GHz. Galangan beban YRA adalah hampir sama dengan 50  $\Omega$  galangan masukan. Hasil kajian juga menunjukkan corak sinaran

menyerupai ragam  $HE_{11}$  bagi keseluruhan julat frekuensi yang dikehendaki. YRA jalur lebar bertindan mempunyai gandaan purata sebanyak 7.49 dB bagi julat frekuensi yang dikehendaki. Kesimpulannya, kerja ini menawarkan YRA yang baik, efisien dan agak mudah dengan menggunakan penyalun YIG lebihan  $Fe_2O_3$  dan persamaan lengkung sesuai yang diubah suai.

# **ANALYSIS OF YTTRIUM IRON GARNET (YIG) RESONATOR WITH EXCESS $\text{Fe}_2\text{O}_3$ FOR WIDEBAND ANTENNA APPLICATIONS**

## **ABSTRACT**

Satellite communications play an important role in telecommunications. Realizing this fact, broadband antennas are part of the solution to establish a concept of wide frequency usage in satellite technology. Wideband dielectric resonator antenna (DRA) provides better efficiency and miniaturization as compared to the metallic antenna. However, having dielectric resonator (DR) with different permittivity ( $\epsilon_r$ ) and size contributes to the increase in the complexity of DRA design and fabrication. Besides, every time to use new dielectric material, it must be fully characterized. This is considered redundant prior to the DRA analysis. Therefore, the intent of this work is to realize efficient wideband antenna and rapid antenna analysis. Improvement to the wideband DRA is done using unbiased low permittivity yttrium iron garnet (YIG) with excess  $\text{Fe}_2\text{O}_3$  to produce cylindrical resonator with the same dimension but different  $\epsilon_r$ . YIG resonator was developed by using solid state reaction method and characterized by x-ray diffraction (XRD), field emission scanning electron microscopy (FESEM) and high performance probe (Agilent 85070E) dielectric probe kit. Based on the characterization result, curve fitting model (CFM) was modified using Minitab software which applies least square method of correlation and regression analysis. Simulations of the YRA structures were carried out using Computer Simulation Technology (CST) Microwave Studio software while measurement of the S-parameters as well as gain were analyzed using the PNA-X



Network Analyzer (8720D, 10MHz-50GHz). The radiation pattern of the YRA was tested by using 10 meter anechoic chamber. XRD and FESEM analysis give indication on fully reacted, dense and solid cylindrical YIG using solid state method. Using different amount of excess  $\text{Fe}_2\text{O}_3$  create low  $\epsilon_r$  YIG within the range of 10.04 to 17.36 with low  $\tan \delta$  value. Correlation between  $\epsilon_r$  and excess  $\text{Fe}_2\text{O}_3$  is used to modify the curve fitting equations. The modified equation provides rapid analysis on YIG antenna by including the presence of excess  $\text{Fe}_2\text{O}_3$  instead of  $\epsilon_r$  value. Correlation coefficient of -0.862 indicates the strong correlation between  $\epsilon_r$  and excess  $\text{Fe}_2\text{O}_3$ . Determination coefficient,  $R^2$  of 99.6% indicates that the curve of the generated equation is fit with  $\epsilon_r$  data. Hypothesis testing with high p-value over 99% verifies that modified equation is well match with the original equations. The fabricated YIG resonators and modified equations are used together to produce wideband stacked YIG resonator antenna (YRA). Three stacked YIG with different combination of excess  $\text{Fe}_2\text{O}_3$  provide the proposed wideband YRA. YIG resonators with excess  $\text{Fe}_2\text{O}_3$  of 8% (YR8), 14% (YR14) and 17% (YR17) present the best YR combinations with frequencies of 17.25 GHz, 19.18 GHz and 20.81 GHz, respectively. The combinational effect of three YIG resonators produces bandwidth of 24.22% measured at -10 dB impedance bandwidth centered at 19.25 GHz. Load impedance of YRA is well-match with input impedance of 50  $\Omega$ . Findings also indicate identical radiation pattern of  $\text{HE}_{11}$  mode throughout the desired frequency range. The stacked wideband YRA has average gain of 7.49 dB over the frequency range. In conclusion this work offers an improved, efficient and relatively simple YRA using YIG resonator with excess  $\text{Fe}_2\text{O}_3$  and modified curve fitting equation.



# CHAPTER 1

## INTRODUCTION

### 1.1 Overview

The space telecommunication technology demands continuous growth in microwave systems to provide high efficiency and gain, wide bandwidth as well as miniaturization capabilities. Broader bandwidth range in such technology is increasing in demand to accommodate multiple channels or single channels with combined information of data such as pictures, audio, and even video therein (Inglls & Luther, 1997). One of the essential elements in microwave system to reach that demand is undoubtedly an antenna. The main characteristic of the antenna is it has wideband capability where it can transmit and receive the radio frequency (RF) signal within a wide range of frequency (Balanis, 2005).

The key factor which affects the overall performance of wideband antenna is its resonating element. Conventional metal type resonator (waveguide and microstrip) has been replaced by dielectric resonator (DR) as the latter offers minimal conduction loss, high stability, lightweight and miniaturization of the microwave devices (Golio & Golio, 2001). The first fabricated DR was rutile material of titanium dioxide ( $\text{TiO}_2$ ) (Sebastian, 2008). Since then extensive experimental and development of DRs such as barium titanate (BT) and zirconium tin titanate ( $\text{ZrSrTiO}_4$ ) had been carried out (Chaudhary et al., 2012a; Chung et al., 2008; Sebastian, 2008). With proper excitation modes and no radiation shielding, DR can actually become efficient antennas. This antenna is specifically known as dielectric resonator antenna (DRA) (Long & O'Connor, 2007).

Using high permittivity DR allows a more compact antenna to be created while low loss tangent ( $\tan \delta$ ) promotes high efficiency especially at millimeter (mm)-wave frequency applications (Sebastian, 2008). Due to enormous potential of this DRA, many extensive studies have been conducted which covers many aspects such as compact design, wideband, tunability and mm-wave frequency applications (Luk & Leung, 2003; Petosa, 2007). To achieve wideband operating antenna using DRA, several methods have been discovered. One of them is by using several DRs within the antenna either in co-planar, stacked or embedded configuration (Luk & Leung, 2003). In wideband DRA by means of multiple DRs, different frequency from the respective DRs are combined together to obtain wideband response. In order to achieve these multiples frequencies, one has to use DRs with different size and from different dielectric material (Wang et al., 2013).

Low permittivity ( $\epsilon_r$ ) DR is favored in wideband DRA because the bandwidth is wider (Petosa, 2007). Amongst the group of low  $\epsilon_r$  materials, yttrium ion garnet (YIG) resonator has attracted a lot of attention due to its inherent features of dual magnetic and dielectric properties (Kulkarni, 2010). When YIG is unbiased in antenna application, it exhibits similar behavior to DRA which is later called as YIG resonator antenna (YRA) (Petosa et al., 1994). Study on the YIG resonator with the presence of electromagnetic source applied in filter, and oscillator is ample (Trew, 1979). However, reports on the application of unbiased YIG resonator for wideband antenna are still scarce. Therefore, study on YRA still need to be investigated and this work has been inspired by the need for simple construction of unbiased YIG, broadband operation and higher efficiency of antenna.

## **1.2 Problem statement**

The demand for an antenna with wideband features to support multiple wireless standards and frequency spectrum keeps on increasing. This can be observed by the increasing trend of multi-functional wireless devices. In satellite communication, wideband antenna play important role to establish a concept of wide frequency usage (Inglls & Luther, 1997). Using several antennas to cover wide frequency range, for instance, from 17.3 GHz to 21.2 GHz for fixed and mobile satellite services causes lot of space and time usage (Commission, 2012). Therefore, a single antenna with wideband characteristic that covers the whole frequency range is the solution for this need. This is to support the full range of domestic and international services encompassing voice, video, data, and other advanced communications services (Conti, 2007).

Normal wideband horn antenna is featured by its metal-made structure. In the satellite communication, it is used as the broadband feeder to the parabolic dish (Othman, 2013). At high frequency, this antenna suffers from high conduction loss. Consequently, the efficiency reduces significantly as the input signal translated into the loss instead of radiated signal (Luk & Leung, 2003). This is also contributed by the surface wave from the metal surface. In order to improve the signal, an amplifier is required in the transponder system. Additionally, metallic antenna is big in size due to their electrical length limitation, thus require a lot of space (Luk & Leung, 2003). The above-mentioned problems can be countered by using DRA with multiple DRs (Petosa, 2007). It is well known that DRA is a low loss antenna which offers high degree of flexibility to adapt with various telecommunication systems (Petosa, 2007). By means of multiple DRs, different frequencies are produced and when combined together it forms a

wideband antenna. To produce dissimilar frequencies, each DR differs from each other in respect of dimension and permittivity ( $\epsilon_r$ ). However, having DRs with different  $\epsilon_r$  and size contributes to the increase in the complexity of DRA design and fabrication. For example, DR with different  $\epsilon_r$  requires different dielectric material in DRA. Fechine et al. (2009) and Chaudhary et al. (2012b) use composite of  $Zr_{0.8}Sn_{0.2}TiO_4$  plus epoxy and  $GdIG_{0.25}YIG_{0.75}$ , respectively to produce DR to obtain wideband stacked DRA. This approach requires additional solid state process to produce DR. Besides, DRs with the same material having different thickness and size were also reported by Fan et al. (1996) and Kumari & Behera (2013) to achieve wideband DRA. Altering the shape of DR is a big challenge due to its inherent hardness (Huang, 2002). That is why there are many reports on the methods to tune the frequency of DRA due to the inconsistency in the size of DR (Leung & So, 2005; Li et al., 1996). Thus, to further improve the DRA efficiency for wideband applications, DRs should have made from the same material with the same dimension.

Improvement to the wideband DRA can be done via innovative material exploitation and modification (Sebastian, 2008). One of the unique materials that have been used extensively in microwave field is YIG (Özgür et al., 2009a; Özgür et al., 2009b). Petosa et al. (1994) proved that YIG can also be utilized as a frequency-tunable antenna. For wideband antenna application, YIG has a big potential to be used as a resonator due to its low  $\epsilon_r$  although it is permeable ( $\mu_r$ ) (Mi et al., 2006). Due to present of permeability property, the usage of YIG is usually accompanied with a big electromagnetic source, resulting in a more complicated antenna design (Petosa et al., 1994). The electromagnetic source is required for biasing purpose to supply static

magnetic field to alter  $\mu_r$  only. Therefore, extra space for placement of the antenna is required, thus raising the difficulty of its fabrication and installation. This will not be the case if  $\epsilon_r$  instead of  $\mu_r$  of YIG is manipulated, such as in the case of Petosa et al., (2009). Therefore, the presence of electromagnetic source can be ignored.

Another important aspect in DRA design is regarding the existing of curve fitting model (CFM) which are only applicable to general purpose analysis of DRA (Kishk & Antar, 2007). The main weakness is that every time to use new dielectric material, it must be fully characterized prior to the DRA analysis. However, this characterization step is considered redundant when similar dielectric materials to be analyzed in DRA design. For example, in the case of dielectric material to have different  $\epsilon_r$ , it can be done through the addition of dopant (Sebastian, 2008). Therefore, the CFM has to be modified by taking into considerations the presence of dopant. Since the amount of dopant added normally is in small quantity, therefore a rapid DRA analysis for this material can be done specifically with the newly modified CFM.

Therefore, in order to realize efficient wideband DRA and rapid DRA analysis, YIG resonator with excess  $\text{Fe}_2\text{O}_3$  can be used. YIG added with various amount of excess  $\text{Fe}_2\text{O}_3$  can produce YIG resonator from the same material but with different  $\epsilon_r$ . By excluding the magnetic source (bar magnet), YIG resonator promotes compactness in antenna application. At the same time, this YIG resonator antenna (YRA) has similar characteristic like a normal DRA where it is only influenced by  $\epsilon_r$  as the external magnetic field is removed. Low  $\epsilon_r$  associated with YIG is suitable for wideband DRA application, since it will enhance the bandwidth of the DRA. Based on the amount of excess  $\text{Fe}_2\text{O}_3$  in YIG, the CFM can be modified. The modification involves substituting

the parameter of  $\epsilon_r$  with the amount of excess  $\text{Fe}_2\text{O}_3$  in YIG. This is very helpful to make rapid analysis on the performance of YRA with no more characterization process is needed. To sum up the aforementioned issues, this study will focus on designing wideband YRA using YIG resonator with different amount of excess  $\text{Fe}_2\text{O}_3$ . A modified CFM will be used to specifically predict the resonant frequency and Q factor of YRA design.

### **1.3 Objectives of research**

The main objective of this research is to study on YIG resonator with excess  $\text{Fe}_2\text{O}_3$  for wideband antenna application. This thesis focuses on the development of a wideband antenna covering required frequency range of 17.3 to 21.2 GHz under Malaysian Communication and Multimedia Commission (MCMC) frequency spectrum's allocations (Commission, 2012) for fixed satellite services (FSS). To accomplish this aim, several objectives have to be achieved. The specific objectives are as follows:

1. To fabricate and characterize YIG with different amount of excess  $\text{Fe}_2\text{O}_3$  in order to produce YIG resonators with same dimension of radius and height but different  $\epsilon_r$ .
2. To model equations for resonant frequency and Q-factor of YIG resonator through modification of original curve fitting model (CFM).



3. To develop wideband stacked cylindrical YRA with excess  $\text{Fe}_2\text{O}_3$  that can cover a wide frequency range from 17.3 GHz to 21.2 GHz. To accomplish this, fabricated YIG with the same dimension and modified CFM are used.

#### **1.4 Scope of Research**

The scope of this project focuses on the design of a microstrip-fed cylindrical stacked YIG antenna. The only microwave resonator used in this design is fabricated from Yttrium Ion Garnet (YIG) via solid state process. Excess  $\text{Fe}_2\text{O}_3$  is added accordingly to the YIG powder to change its properties. All YIG resonators are fabricated in cylindrical form with radius and height that is identical to each other. These YIG resonators are characterized to determine its  $\epsilon_r$  and  $\tan \delta$  value. Curve fitting model (CFM) was modified using least square method to include the influence of excess  $\text{Fe}_2\text{O}_3$ , instead of  $\epsilon_r$ . Together with fabricated YIG resonators, modified CFM is used in the stacked YIG antenna design. Simulation of the stacked YIG antenna was carried out by using Computer Simulation Technology (CST) Microwave Suite 2013 software. From the simulation, the performance of the proposed antenna could be fully understood and optimized. The proposed antenna is excited directly by a microstrip line which is photo etched on the microwave substrate from Roger Corporation RO4003C. It has  $\epsilon_r$  of 3.38, thickness of 0.813 mm, and  $\tan \delta$  of 0.0027. In the end, comparisons are made between the simulation from CST and measurement results in term of S-parameter, radiation

pattern and gain to ascertain the degree of agreement. These results were analyzed, discussed, and conclusions were drawn based on the observations.

## **1.5 Contributions**

The completed work has four main contributions.

- i. Fabrication of YIG resonator with excess  $\text{Fe}_2\text{O}_3$  through modification of YIG stoichiometric formulation to produce cylindrical YIG that has the same dimension but different  $\epsilon_r$  using solid state method.
- ii. Characterization of  $\epsilon_r$  and  $\tan \delta$  for YIG resonator with various excess  $\text{Fe}_2\text{O}_3$  from 5 GHz to 25 GHz.
- iii. The CFM for resonant frequency and Q factor were modified and adapted for the proposed wideband YIG antenna. These modified equations are exclusively for the analysis of YIG resonator with excess  $\text{Fe}_2\text{O}_3$ .
- iv. The development of wideband stacked cylindrical YRA using the fabricated YIG with excess  $\text{Fe}_2\text{O}_3$  and modified equations. This antenna operates at 17.3 GHz to 21.2 GHz suitable for fixed satellite communications

## **1.6 Thesis Organization**

The thesis has been divided into a total of five chapters. Chapter 1 outlines the problem statements, expected goals, scope and contribution of the study.

Chapter 2 presents the features of microwave resonator and intensive literature review on YIG in antenna application. Model analysis used to predict the resonant frequency and Q factor are also discussed here. The concept on statistical analysis of antenna using least square methods is also explained in details. Reviews of available methods to enhance impedance bandwidth of antenna especially for stacked configuration are also presented.

Chapter 3 contains detailed description of experiments carried out. This includes solid state fabrication process of YIG resonator and its characterization analysis. Statistical method used to modify the curve fitting equation for YIG antenna is explained in this chapter. Detailed description of the YIG antenna design including the microstrip line structure, real dimension of YIG resonator and number of stacks involved was also presented. Simulation procedure which was carried out using CST software and measurement of  $S_{11}$  as well as radiation pattern are also presented.

Chapter 4 discusses in details the result of YIG resonator characterization and modified curve fitting equation generated from the characterization data. The simulation results in terms of input impedance, S-parameter and radiation pattern have been generated for wideband antenna. Comparison is then made between measurement and simulation results. Analysis on the investigation of the coupling and structure variation of YIG resonator is also done. Finally, Chapter 5 discusses the achievements of the thesis, and recommendation for future works based on limitation of the research.

## CHAPTER 2

### LITERATURE REVIEW

#### 2.1 Dielectric Resonator

##### 2.1.1 Introduction

Dielectric resonator (DR) is a resonator fabricated from low loss dielectric material that can be used in microwave circuit. Figure 2.1 shows cylindrical DR used in the microwave circuit with diameter of  $2a$  and height of  $h$ . In 1939, dielectric material in the form of unmetallized dielectric object was first introduced theoretically able to act as a resonator (Richtmyer, 1939). Only after 30 years of its discovery, low-loss DR known as barium tetratitanate ( $\text{BaTi}_4\text{O}_9$ ) was successfully fabricated which paved the way for the use of DR as high Q element in filters, antennas and oscillators (Long & O'Connor, 2007; Sebastian, 2008).

It can function as a resonator due to the internal reflection of electromagnetic wave at the high  $\epsilon_r$  material/air boundary to form a resonant structure. This results in confinement of energy within and in the vicinity of the dielectric material and forms a standing wave. This standing wave has a specific field distribution pattern or mode at a particular frequency (Long & O'Connor, 2007; Golio & Golio, 2001). The level of energy confined inside the resonator is dependent on  $\epsilon_r$  (Golio & Golio, 2001). In DR, some parts of the microwave will leak when the wave moves through high  $\epsilon_r$  dielectric material to low  $\epsilon_r$  of air. The leakage fields from the resonator can be used for coupling purpose, tuning the frequency and transmitting the microwave signal (Chi & Zaki, 2007; Long & O'Connor, 2007; Golio & Golio, 2001).

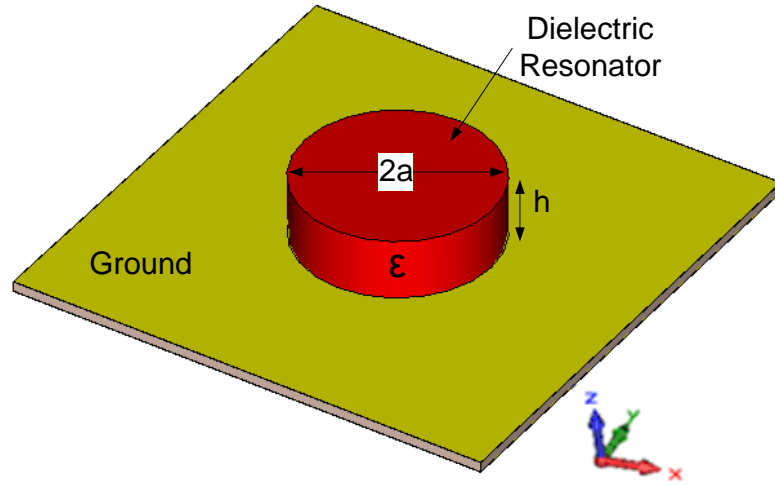


Figure 2.1: Cylindrical dielectric resonator structure

### 2.1.2 Major Features

Dielectric resonator (DR) is famously known for its high degree of flexibility and versatility, allowing for designs to suit any communication applications (Petosa, 2007). The features which are general to most DRs making it extensively useful in microwave devices are:

a) The size of DR can be controlled by means of  $\epsilon_r$  of the dielectric material. By increasing the  $\epsilon_r$  of DR, the size of DR reduces and vice versa (Sebastian, 2008). Increasing  $\epsilon_r$  also reduces the bandwidth of DR. The  $\epsilon_r$  can be varied ranging from 8 to 100, thus allowing more control over the size and bandwidth of DR (Petosa, 2007; Petosa & Ittipiboon, 2010).

b) There is a minimal dissipation loss and nonexistence of surface wave losses in DR. It is because DR is fabricated from low-loss material and not from conducting material. It leads to high efficiency DR especially at mm-wave frequency where the conduction loss becomes high (Luk & Leung, 2003). In comparison to DR, metal-type resonators such as metallic waveguide and patch resonators suffer from conduction loss severely as frequency increase (Qinghua et al., 2008).

c) Coupling to DR can be done by using various feeders such as probes, slots, microstrip lines, and coplanar waveguide. This enables DR to be easily integrated into any existing technology. Then, various modes ( $TE_{01}$ ,  $TM_{01}$  and  $HE_{11}$ ) can be excited through different feeding mechanism. The type of feeder and its location are very essential to generate the desired mode in DR. This, in turn generates the input impedance and radiation characteristic of DR (Kajfez & Guillon, 1986; Petosa, 2007).

d) Different shapes of DR can be formed into cylinders, rectangles and hemispheres. Additionally, it can also be fabricated into a more complex shape such triangle, and trapezoid. Each shape of DR has its own aspect ratio to provide platform to control the parameter of length, height, width and radius. Complex shape of DR with many edges and corners offer greater design flexibility (Petosa et al., 1998).

### 2.1.3 Methods of Coupling

One of the features of DR is that various feeding mechanism of microstrip line (Kranenburg & Long, 1988), probe (Kishk, 2001), slot (Mongia et al., 1993), coplanar waveguide (Kranenburg et al., 1991) and dielectric image waveguide (DIG) (Wyville et al., 2005) can be used to excite it efficiently. Table 2.1 shows the advantages and disadvantages of various coupling methods in DR. Out of all feeders, microstrip line coupling is most suitable in this research due to its simplicity, facilitates integration with other microwave circuits and for general study of DR (Rashidian et al., 2013; Kumar Mongia & Ittipiboon, 1997). Figure 2.2 illustrates the diagram for each feeding mechanism of DR.

Table 2.1: List of coupling methods for DR

Type of Feeder	Advantages	Disadvantages
Probe	Direct straight 50 $\Omega$ coupling	Need to drill a hole, thus introduce air gap between the probe and DR
Slot	Isolate the radiating aperture (slot) from any unwanted coupling.	Not applicable at high frequency as the slot size becomes small and can generate multiple higher modes.
Microstrip line	Facilitate integration with other microwave circuits and array configurations. Simplest feeder among the coupling method	Influence of the connector into radiating element especially at high frequency.
Coplanar waveguide	Additional control for impedance matching	Higher conduction loss due to additional copper area around the resonator
Dielectric image waveguide (DIG)	Good at millimeter wave frequency and best utilized as series feed to a linear array	Not low profile and occupies extra space contributing to more complex design

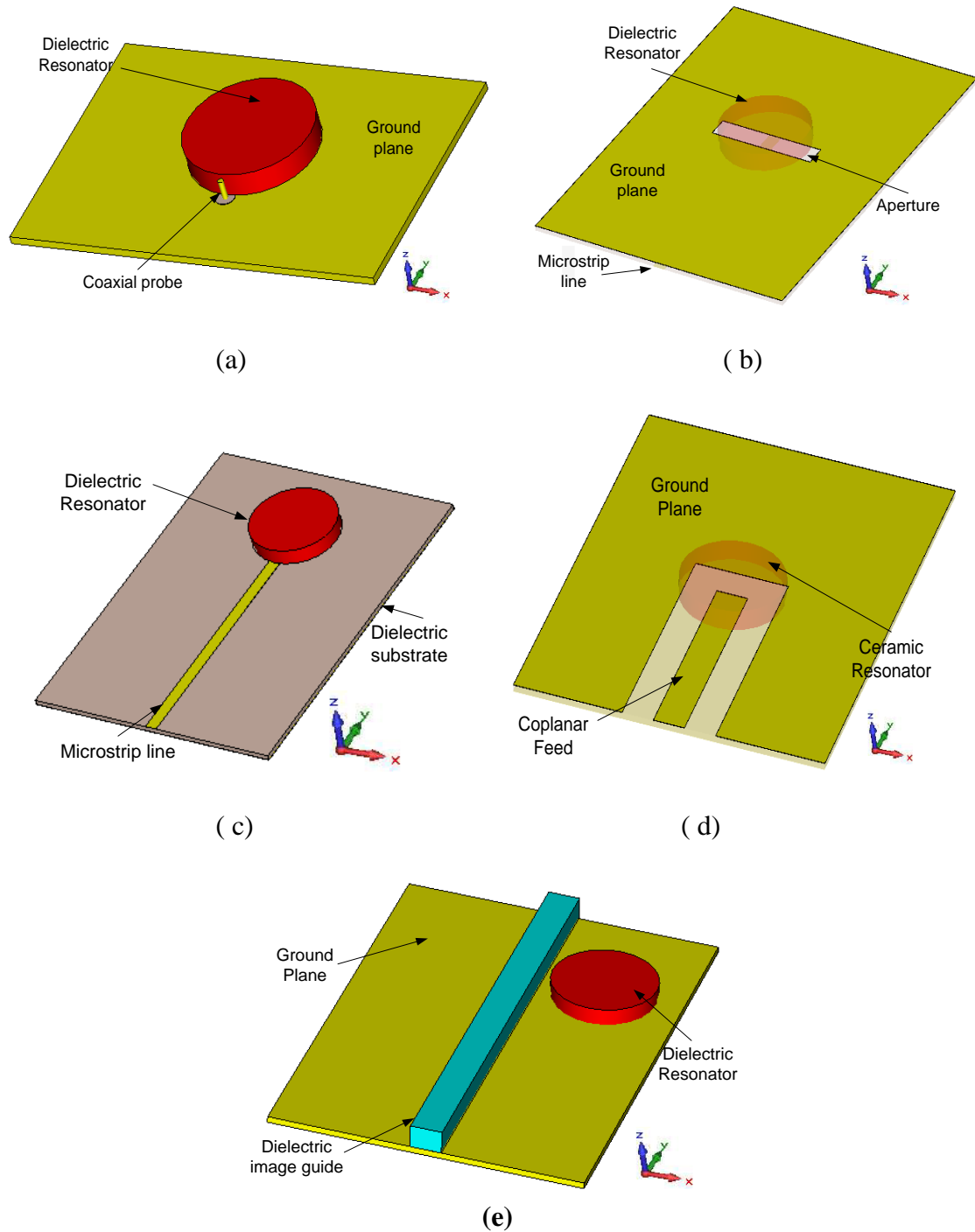


Figure 2.2: Methods of coupling (a) Probe coupling, (b) Slot coupling, (c) Microstrip line coupling, (d) Coplanar waveguide coupling, and (e) Dielectric image guide (DIG) coupling



#### 2.1.4 The Significance of Electromagnetic Field Pattern

Knowledge on the field pattern is very useful in designing DR for certain applications. Firstly, it will give the know-how to accurately couple the DR to achieve a desired mode based on particular field distribution pattern (Petosa, 2007). Equation 2.1 states that, strong coupling is obtained when the electric current source (probe) is located in an area of strong electric field within the DR. On the other hand, to achieve strong coupling using magnetic current source (loop), then from Equation 2.2 the source should be located in an area of strong magnetic field. The amount of coupling,  $\chi$ , between the source and fields within the DRs can be determined from the amounts of electric,  $E_{DR}$  and magnetic,  $H_{DR}$  fields using the Lorentz Reciprocity Theorem and coupling theories (Collin, 1966).

$$\chi \propto \int_V (E_{DR} J_s) dV \quad (2.1)$$

$$\chi \propto \int_V (H_{DR} M_s) dV \quad (2.2)$$

where  $J_s$  and  $M_s$  are electric and magnetic sources respectively and  $V$  is the volume occupied by the source within the electric and/or magnetic currents. A feeder can generate different modes depending on the placement of the feeder to the cylindrical DR. For instance, probe feeder located at the edge of cylindrical DR resulted in  $HE_{11}$  mode, while putting it at the center, excites  $TM_{01}$  (Kajfez & Guillon, 1986).

Secondly, the knowledge of internal field distribution of DR provides guideline in designing proper frequency tuning mechanism (Kajfez & Guillon, 1986). Based on

Equations 2.1 and 2.2, in order to obtain large frequency tuning, the perturber (tuning screw, varactor etc) should be placed in DR where the electric/magnetic current source is the strongest. If the disturber is placed in an area of weak electric/magnetic field, then there will be less frequency tuning (Chi & Blair, 2002; Virdee, 1997). Figure 2.3 shows a varactor diode that is placed near to the dielectric resonator to disturb the magnetic field and thus the frequency. DC power supply is used to tune the frequency of DR for different DC values.

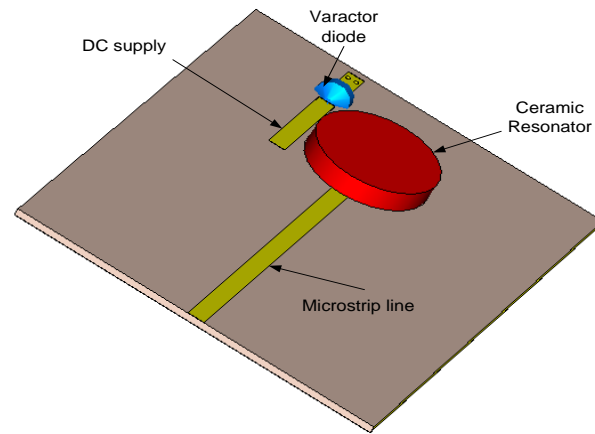


Figure 2.3: Tunable DR with varactor diode.

Thirdly, by observing the magnetic/electric field pattern in DR, one might propose a mode suppression device for particular modes (Karp et al., 1968; Tan & Helszajn, 1976). For instance,  $HE_{11}$  mode is suppressed by wrapping two wires around the DR at right angles in package styles such as shown in Figure 2.4. The mode is suppressed because the wires conductor forces the electric field tangential to the top, bottom and sides of DR to zero along the wires line (Karp et al., 1968). However, presence of these wires does not significantly affect the  $TE_{01}$  mode.

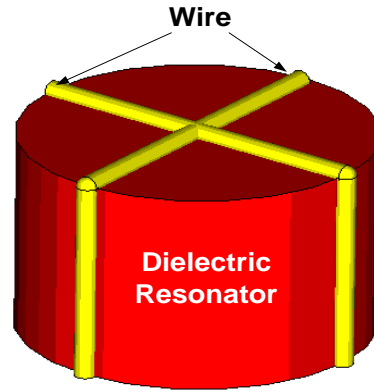


Figure 2.4:  $HE_{11}$  mode suppression method of cylindrical DR.

### 2.1.5 Excited Modes Using Microstrip line Coupling

Coupling to dielectric resonator (DR) by means of microstrip line can excite modes of TM, TE and HE depending on the position of DR to the microstrip line. The TE and TM modes are axially symmetric with no azimuthal dependence while the hybrid mode of HE has dependence on azimuth (Petosa, 2007). The modes which are most commonly used for radiating applications are the  $TM_{01\delta}$ ,  $TE_{01\delta}$  and  $HE_{11\delta}$  modes. The modes are differentiated based on the subscripts which refer to field variations in the azimuth ( $\phi$ ), radial ( $r$ ), and axial ( $z$ ) directions in cylindrical coordinate. The value of  $\delta$  ranges from zero and approaches one for high values of  $\epsilon_r$ . Since  $\delta$  is seldom needed, hence, DR normally is defined by the first two indexes only (Kajfez & Kishk, 2002).

By using curved microstrip line such as shown in Figure 2.5, proper magnetic coupling is generated to form  $TE_{01}$  mode inside DR. The pattern of electric field is like a circular circle around the cylinder DR. It is strong everywhere except at the centre of cylindrical DR. The resulting fields of cylindrical DR for  $TE_{01\delta}$  mode with any kind of

coupling methods on a ground plane is shown in Figure 2.6 (Kajfez & Guillon, 1986). For magnetic field of  $TE_{01}$  mode, it is strong down the center of cylindrical DR (Kajfez & Guillon, 1986). This electromagnetic field distribution indicates that the removal of the center part of DR (doughnut shape) will not significantly change the resonant frequency in DRA. This characteristic has prompt many researchers to study how to control the frequency of ring DR by inserting metal rod at the center of the resonator (Qing-Xin et al., 2013).

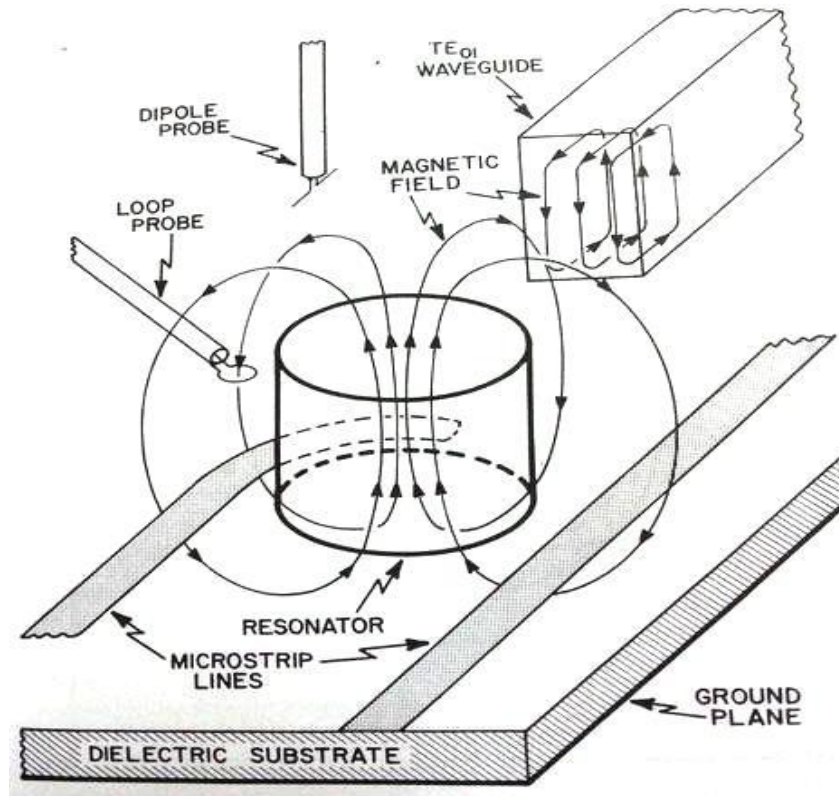


Figure 2.5: Method of coupling to  $TE_{01}$  DR (Kajfez & Guillon, 1986).

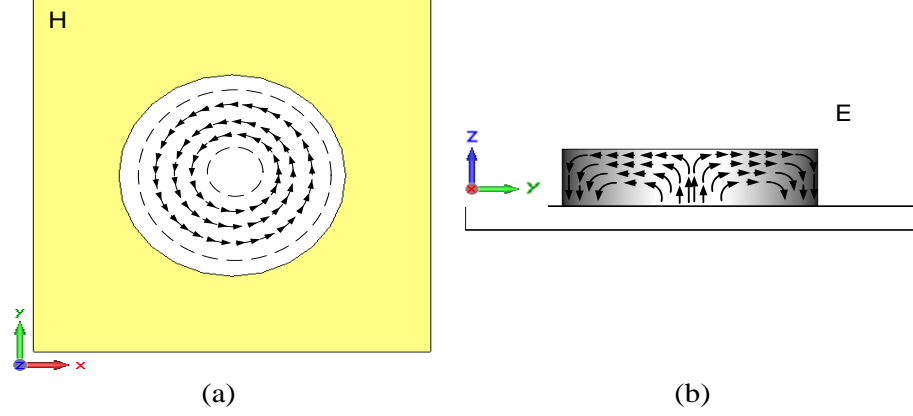


Figure 2.6: Field distribution of the  $TE_{01\delta}$  mode: (a)  $H_x$  and  $H_y$  at  $z = 0$ ; (b)  $E_y$  and  $E_z$  at  $x = 0$  (Othman, 2013)

The fields of  $TE_{01}$  mode can be approximated by the following Equations 2.3 to 2.6 (Petosa, 2007).

$$H_z \propto J_0(\beta r) \cos\left(\frac{\pi}{2h} z\right) \quad (2.3)$$

$$H_r \propto J_1(\beta r) \sin\left(\frac{\pi}{2h} z\right) \quad (2.4)$$

$$E_\phi \propto J_1(\beta r) \cos\left(\frac{\pi}{2h} z\right) \quad (2.5)$$

$$E_z = E_r = H_\phi = 0 \quad (2.6)$$

where  $J_0(\beta r)$  and  $J_1(\beta r)$  are Bessel functions of the first type, and  $\beta$  is a solution of  $J_0(\beta a) = 0$ , where  $a$  is the radius of the cylindrical DR.

In  $TM_{01}$  mode, the fields are similar to those of the  $TE_{01}$  with the magnetic and electric field components interchanged. To generate this mode by using microstrip line, DR is placed by its side on the microstrip line so that the magnetic field lines loop is

parallel to the surface of DR. It can also be excited by means of probe when the probe is placed at the center of DR. Electric field is strong only along the axis and center of DR while the magnetic field is well-contained near the top and bottom faces of DR and forming a circular circle (Kajfez & Guillon, 1986). Figure 2.7 illustrates the placement of different feeders to excite this mode.

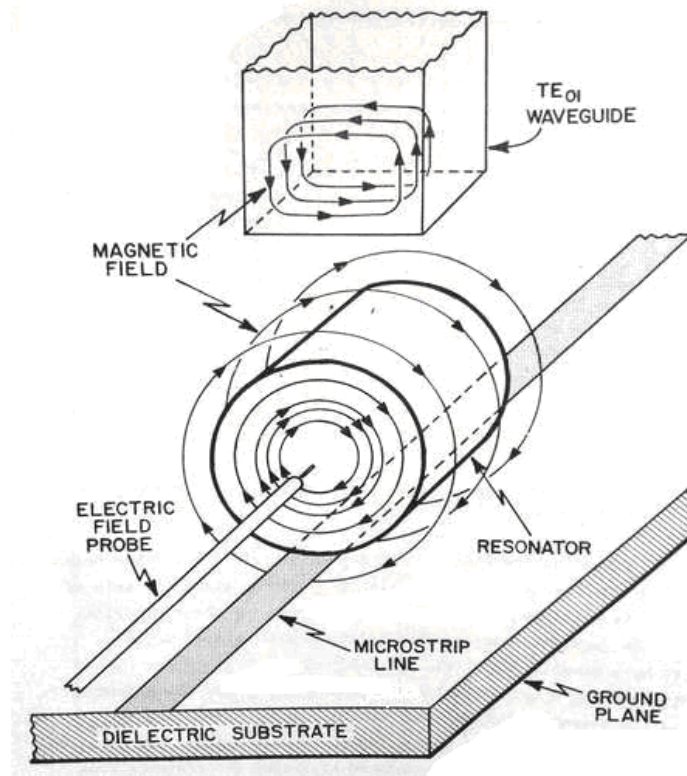


Figure 2.7: Method of coupling to  $TM_{01}$  DR (Kajfez & Guillon, 1986).

$HE_{11}$  mode can be excited by microstrip line feeder if the position of DR is placed flatly at the end of an open microstrip line such as shown in the Figure 2.8(a). The amount of coupling is controlled by adjusting the spacing between the dielectric resonator and line for side-coupling configuration. For the case of direct-coupling, this is done on the length of the line underneath the DR which is represented by  $s$  (Petosa,

2007). Apart from microstrip line,  $HE_{11}$  mode can also be excited via slot and probe feeder such as shown in Figure 2.8(b). The electric field of  $HE_{11}$  mode is the strongest at the side and top of DR but weak at the center. The same goes to the magnetic field but in an opposite direction of  $90^\circ$  to electric field (Kajfez & Guillon, 1986). The resulting field of  $HE_{11}$  mode for cylindrical DR is shown in Figure 2.9.

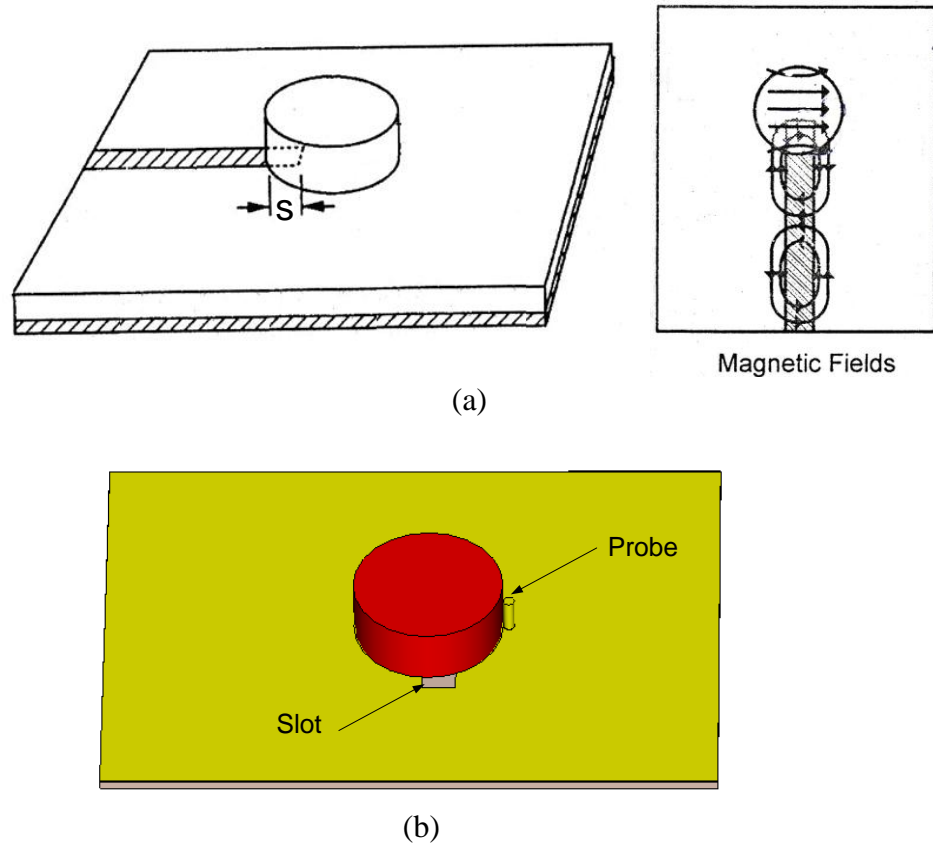


Figure 2.8: Coupling to  $HE_{11}$  mode: (a) microstrip line; (b) probe and slot coupling to  $HE_{11}$  mode (Petosa, 2007).

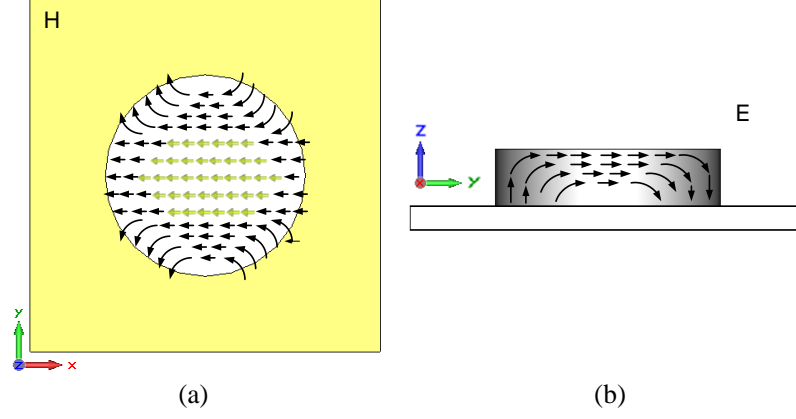


Figure 2.9: Field distribution of  $HE_{11\delta}$  mode: (a)  $H_x$  and  $H_y$  at  $z = 0$ ; (b)  $E_y$  and  $E_z$  at  $x = 0$  (Othman, 2013)

This field component of  $HE_{11}$  mode can be expressed in the form of Equations 2.7 to 2.12 (Petosa, 2007):

$$E_z \propto J_1(\alpha r) \cos\left(\frac{\pi}{2h} z\right) \begin{cases} \cos \phi \\ \sin \phi \end{cases} \quad (2.7)$$

$$E_r \propto \frac{\partial J_1(\alpha r)}{\partial(\alpha r)} \sin\left(\frac{\pi}{2h} z\right) \begin{cases} \cos \phi \\ \sin \phi \end{cases} \quad (2.8)$$

$$E_\phi \propto J_1(\alpha r) \sin\left(\frac{\pi}{2h} z\right) \begin{cases} \sin \phi \\ \cos \phi \end{cases} \quad (2.9)$$

$$H_r \propto J_1(\alpha r) \cos\left(\frac{\pi}{2h} z\right) \begin{cases} \sin \phi \\ \cos \phi \end{cases} \quad (2.10)$$

$$H_\phi \propto \frac{\partial J_1(\alpha r)}{\partial(\alpha r)} \cos\left(\frac{\pi}{2h} z\right) \begin{cases} \cos \phi \\ \sin \phi \end{cases} \quad (2.11)$$

$$H_z \approx 0 \quad (2.12)$$

where  $\alpha$  is the solution for  $J_1(\alpha a) = 0$  and the location of the feed influences the choice of  $\cos \phi$  or  $\sin \phi$  while  $a$  and  $h$  are radius and height of the dielectric respectively.



## 2.2 YIG Resonator

### 2.2.1 Overview

Yttrium iron garnet (YIG) is a group of dielectric material. It has a general formula of  $Y_3Fe_5O_{12}$  where Y, Fe and O represent elements of yttrium, iron and oxygen, respectively. It is a well-known material in the group of silicate mineral or garnet. Garnet, spinel and hexaferrite are three different crystal structures in ferrite or ferrimagnetic material (Valenzuela, 1994; Goldman, 2006).

In YIG structure, there are three kinds of cation sites of tetrahedral, octahedral, and dodecahedral. Two and three iron ions ( $Fe^{2+}$ ,  $Fe^{3+}$ ) occupy octahedral and tetrahedral sites, respectively while trivalent yttrium ions ( $Y^{3+}$ ) occupy the largest site of dodecahedral such as shown in Figure 2.10. Each site shares same edges and corners through oxygen atoms (Valenzuela, 1994). Dodecahedral and octahedral ions are parallel to each other, hence there is no magnetic moment. In contrast, tetrahedral cations are in antiparallel orientation with octahedral cations resulting in net magnetic moment. Therefore, the properties of YIG are due to the  $Fe^{3+}$  ions not  $Y^{3+}$  ions (Özgür et al., 2009a; Valenzuela, 2012; Goldman, 2006).

All the microwave properties of YIG are generated from these three cation sites. Four mechanisms that trigger ferrimagnetic characteristics are domain wall bowing, domain wall displacement, spin rotation and spin waves (Valenzuela, 1994). While  $\epsilon_r$  of YIG is due to the presence of large oxygen ions insulating metal ions in the crystal structure (Valenzuela, 2012). Therefore, they are also in the group of dielectric that is hard and poor electrical conductors. The simplest method to produce YIG material is via

classic solid state reaction (Cortés-Escobedo et al., 2013). Besides, YIG can also be produced using sol-gel and combustion synthesis in order to lower the sintering temperature and improve the purity of the YIG (Öztürk et al., 2009; Vajargah et al., 2008).

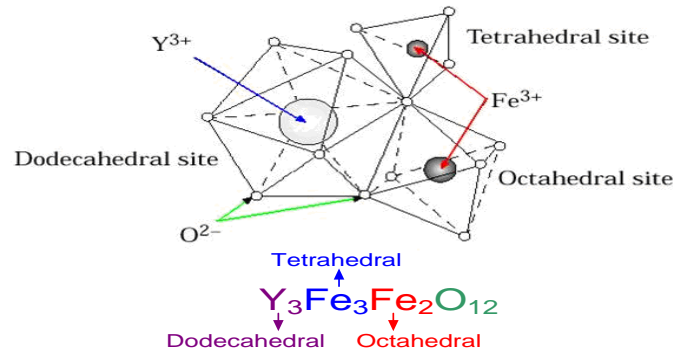


Figure 2.10: Crystal structure of YIG garnet (English, 2014)

YIG ceramic was used in RF devices as passive components (isolator, circulator, antenna and filter) (Adam et al., 2002). However, it is also useful in active devices such as oscillator. YIG oscillator was used extensively to provide high Q factor, broadband characteristics and linear tuning elements (Trew, 1979). In YIG isolator, the incident electromagnetic wave propagates smoothly from input to output port, while the wave is totally attenuated when it moves the other way around (Valenzuela, 2012). YIG circulator provides easy isolation between different channels of a microwave circuit in radar and radio link application. Besides, YIG was used in phase shifter and waveguide applications (Özgür et al., 2009b). However, based on a number of studies, application of YIG in antenna application is still less due to the presence of electromagnet for DC biasing hinders its development (Petosa et al., 1994; Fehine et al., 2008; Zervos et al., 2012).